Prototype fcc-based binary-alloy phase diagrams from tight-binding electronic-structure calculations

P. Turchi,* M. Sluiter, and D. de Fontaine
Department of Materials Science and Mineral Engineering, University of California, Berkeley, California 94720
(Received 27 January 1987)

The generalized perturbation method (GPM), previously introduced to investigate the relative stability of simple and complex structures at $T=0$ K for transition-metal alloys, is applied to the calculation of fcc-based order-disorder phase diagrams with the use of the cluster-variation method (CVM). Results obtained with the GPM have shown that it was possible to expand the electronic configurational contribution of the total energy, namely the ordering energy, as a sum of concentration-dependent effective cluster interactions, taking the completely disordered state as a reference medium. These interactions are computed from a simple but realistic description of the electronic structure based on the tight-binding approximation appropriate for transition-metal alloys. Calculated energies of mixing and effective interactions are then introduced into the CVM free energy, thereby leading to the calculation of prototype phase diagrams describing phase equilibrium between fcc superstructures of type $L1_0$ and $L1_2$ and the corresponding disordered phase. Electronic parameters are varied systematically and their influence on the topology of the resulting phase diagrams is studied for the first time.

I. INTRODUCTION

Experimental phase diagrams of binary substitutional alloys, in which both components are transition metals, are now available for most of the systems, although this information is often not completely known. One can deduce from these diagrams that these alloys show a wide variety of atomically ordered structures stable at low temperatures.

The computation of the coherent phase diagrams (i.e., those for which all phases are either the parent lattice or its superstructures) in binary alloys $A_{1-c}B_c$ has been extensively studied by means of statistical models involving phenomenological cluster interactions.[1] Most of these calculations are based on pairwise interactions; nevertheless, since these interactions are usually assumed to be concentration independent, the phase diagram is necessarily symmetric about $c=\frac{1}{2}$. One way to make the results more realistic is to include multisite interactions; the general asymmetry of the phase diagram is then restored.[2]

It is not clear, however, how one must go about calculating those concentration-independent cluster interactions from microscopic, i.e., electronic theory. Furthermore, the convergence of the cluster expansion is not assured. Hence, in the present investigation, an expansion of the configurational contribution to the internal energy is preferred and performed about a state of complete disorder, the expansion coefficients, or effective interactions, then being necessarily concentration dependent. Such is the spirit of the Ducastelle-Gautier generalized perturbation method (GPM).[3] The outline of the present study is the following: in Sec. II we review briefly the GPM applied to paramagnetic transition metals, using a simple but realistic tight-binding scheme; the formalism is presented and described in order to introduce the electronic parameters required in the following sections. In Sec. III we discuss, on an elementary level, the general properties of the effective pair interactions previously introduced. Although the alloy model is simple, it provides a great deal of information. We will show in Sec. IV that the results obtained at $T=0$ K, in relation with the problem of finding the ground states of the Ising model, allow us to understand the general tendencies for ordering or phase separation depending on a set of relevant electronic parameters. In Sec. V we define the free-energy model in a way consistent with both the GPM and the Kikuchi cluster-variation method (CVM). In Sec. VI we apply this general approach to the calculation of prototype fcc-based order-disorder phase diagrams. We will see that even within the tetrahedron approximation of the CVM and first-neighbor effective pair interactions (V_1) alone, it is possible to generate a wide variety of phase diagrams: the results will be discussed for each set of electronic parameters. Finally, in Sec. VII some concluding remarks will be made.

At the beginning we mentioned the necessity of developing a microscopic model in order to have a clear insight into the nature of the pair and, more generally, cluster interactions, quantities which are very often considered as phenomenological parameters in the statistical models. In the particular case of transition-metal alloys, because of the strong d character of the electrons, specific problems appear. In this respect the pseudopotential theory, reliable for almost free electrons, and which is commonly used to expand the cohesive energy in terms of pair interactions,[4] gives a poorly convergent series in the case of transition-metal alloys. As was emphasized by Friedel,[5] this is mainly due to the large contribution of multiple interactions to the total energy, large compared to that of pair interactions. Although the cohesive energy of transition metals and alloys could not be expressed as a sum of pair potentials, the ordering energy of an alloy, i.e., the energy difference between a (partially) ordered state and

that of complete disorder, could, following the pioneering ideas of Ducastelle and Gautier,[3] be expanded as a sum of effective pair and cluster interactions.[6-11] The main idea of this approach, called the GPM, is to apply a perturbation theory to a reference medium, characterized by $E_{\rm ref}$, which is closely related to a particular configuration of the alloy, at a given concentration. As it was proved, the completely disordered medium, such as the one described by the Soven-Taylor coherent-potential approximation (CPA), whose volume is nearly that of the configuration in question, forms a suitable reference medium. To be valid the theory must take into account, on the one hand, the finite lifetime of the electronic states which specify the reference medium and, on the other hand, the possible large difference between the potentials v_i $(i=A,B)$ of the two components of the alloy, since very often the most stable ordered structures are encountered for large electronegativity or e/a ratio differences.

Let p_n^i be the occupation numbers usually defined as $p_n^i=0$ or 1 depending on whether site n is occupied or not by an atom of type i $(i=A,B)$. Thus for a binary alloy $A_{1-c}B_c$, in which only chemical rearrangements exist, each atomic configuration is completely characterized by the set $\{p_n^i\}$. By use of the GPM, the band energy $E(\{p_n^i\})$ of a given configuration $\{p_n^i\}$ of the alloy can be written as a sum of two terms: (i) the energy of the totally disordered state, which is concentration dependent and configurationally independent, $E(\{c_i\})$, also called the disordered energy $E_{\rm dis}(c)$, (ii) the ordering energy $\Delta E_{\rm ord}(\{p_n^i\})$ which is the difference between the energy of the ordered state specified by the set $\{p_n^i\}$ (this term is also called configurational energy) and the energy of the totally disordered state.

Thus the band energy is given by

$$E(\{p_n'\})=E_{\rm dis}(c)+\Delta E_{\rm ord}(\{p_n^i\}) ,$$

with

$$\Delta E_{\rm ord}(\{p_n^i\}) = \sum_{l=1}^{\infty}\frac{1}{l}\sum_{\substack{n_0\neq n_1\\ n_1\neq n_2\\ \vdots\\ n_{l-1}\neq n_0}} V^{(l)}_{n_0 n_1\cdots n_{l-1}}\,\delta c_{n_0}\delta c_{n_1}\cdots\delta c_{n_{l-1}} ,$$

where $\delta c_{n_j}=p_{n_j}-c$ is the concentration deviation at site n_j, and p_{n_j} refers, here and subsequently, to the B atom occupancy.

These cluster interactions, for a given lattice (fcc, bcc, hcp, $A15$,...), depend upon the distances between the cluster sites n_j and their relative arrangements, the concentration c $(\equiv c_B)$, and the following electronic quantities: the Fermi energy $\bar{\varepsilon}_F$ which determines the filling of the band with respect to the completely disordered state, i.e., the average number of electrons per atom, and the chemical disorder through the one-electron potential difference v_A-v_B. Note that the concentration dependence of the cluster interactions reflects the properties of the reference medium and, therefore, the average local neighborhood of the clusters. Due to mean-free path effects, we expect a rapid convergence of the expansion since the value of the chemical disorder is large.

A major advantage of the GPM is that the ordering energies, which can be calculated for absolute zero of temperature, completely specify the ordered superstructure of the given parent lattice. The determination of the most stable homogeneous ordered structures then reduces to a search of the ground states of the generalized three-dimensional Ising model, for which solutions are known in a number of cases. (See, for example, Refs. 12 and 13.) Furthermore, as will be shown later, for phase equilibrium determination at higher temperatures, the GPM allows the 0-K electronic-structure calculations to decouple from local-order effects which are temperature dependent. To gain qualitative understanding of the effects of electronic parameters on the stability of ordered structures and on the topology of phase diagrams, we shall investigate the properties of these effective interactions in the case of paramagnetic transition-metal alloys by means of the tight-binding approximation (TBA).

II. FORMALISM

As usual, we assume that the most important properties of a given transition-metal alloy $A_{1-c}B_c$ come from the d band. Thus we will adopt the following tight-binding Hamiltonian to describe the alloy in a particular configuration $\{p_n^i\}$:

$$H=h+V ,$$

with

$$h=\sum_{n,\lambda}|n,\lambda\rangle\sigma_n\langle n,\lambda|+H_0 ,$$

$$V=\sum_{n,\lambda}|n,\lambda\rangle(\varepsilon_n-\sigma_n)\langle n,\lambda| ,$$

where we have the following:

(i) H_0 is the Hamiltonian of the pure metal:

$$H_0=\sum_{\substack{n,m\neq n\\ \lambda,\mu}}|n,\lambda\rangle\beta_{nm}^{\lambda\mu}\langle m,\mu| .$$

(ii) σ_n is the self-energy centered on site n and $\varepsilon_n=\sum_i p_n^i\varepsilon_i$ $(i=A,B)$: ε_i being the energy of the atomic level associated with the species i (we neglect crystalline field effects for simplicity).

(iii) n and m are lattice sites, λ and μ are orbital labels (here $\lambda,\mu=1,2,\ldots,5$ corresponding to the five atomic d orbitals).

The $\beta_{nm}^{\lambda\mu}$ are hopping integrals, which, according to the simplest scheme, can be expressed in terms of three parameters only: $(dd\sigma)$, $(dd\pi)$, and $(dd\delta)$.[14] For the sake of simplicity, we will neglect the dependence of the $\beta_{nm}^{\lambda\mu}$ on the nature of the species located at sites n and m.

The σ_n, for which the orbital dependency can be neglected in a first step, are calculated by using the self-consistent relation given in the CPA formalism by

$$\sum_i c_i t_n^i = 0 ,$$

where t_n^i is the diffusion potential of an electron in the effective reference medium on a site n occupied by an atom of type i. The so-called t matrix is given by

$$t_n^i = \frac{\varepsilon_i - \sigma_n}{1-(\varepsilon_i - \sigma_n)F_n}, \quad F_n = \tfrac{1}{5}\sum_\lambda F_n^\lambda$$

where F_n^λ is the diagonal matrix element of the CPA Green's function. If G_0 is the resolvent associated with H_0, then F, in operator notation, is expressed as

$$F(z) = G_0(z-\sigma(z)) .$$

In this simple description the ordering energy $\Delta E_{\rm ord}(\{p_n^i\})$ becomes[9,11]

$$\Delta E_{\rm ord}(\{p_n^i\}) = \frac{1}{N}\sum_{n,i}(p_n^i - c_i)h_n^i + \frac{1}{2N}\sum_{\substack{n\neq m \\ i,j}}(p_n^i - c_i)(p_m^i - c_j)V_{nm}^{ij} + \cdots , \tag{1}$$

with

$$h_n^i = \frac{1}{5\pi}\mathrm{Im}\int_{-\infty}^{\bar\varepsilon_F} dE \sum_\lambda \ln[1-(\varepsilon_i-\sigma_n)F_n^\lambda] ,$$

$$V_{nm}^{ij} = -\frac{1}{5\pi}\mathrm{Im}\int_{-\infty}^{\bar\varepsilon_F} dE\, t_n^i t_m^j \sum_{\lambda,\mu}(\bar G_{nm}^{\lambda\mu})^2 ,$$

where $\bar\varepsilon_F$ is the Fermi energy of the disordered alloy described within the CPA, N is the total number of atoms, and $\bar G_{nm}^{\lambda\mu}$ is the partial interatomic (or off-diagonal) matrix element of the CPA Green's function.

The general expression (1) has been shown to converge rapidly in most cases. It applies to any crystalline structure but becomes particularly simple when all sites are equivalent, then σ_n, F_n^λ, t_n^i, and h_n^i no longer depend on n and the first term on the right-hand side of (1) vanishes. Then, to the lowest approximation, we are left with effective pair interactions (EPI) only and expression (1) is written as

$$\Delta E_{\rm ord}(\{p_n\}) \simeq \frac{1}{2N}\sum_{n\neq m}(p_n - c)(p_m - c)V_{nm} , \tag{2}$$

where p_n stands for p_n^B and V_{nm} is the EPI between sites n and m given by

$$V_{nm} = V_{nm}^{AA} + V_{nm}^{BB} - 2V_{nm}^{AB} ,$$

with

$$V_{nm} = -\frac{1}{5\pi}\mathrm{Im}\int^{\bar\varepsilon_F} dE\,(\Delta t)^2 \sum_{\lambda,\mu}(\bar G_{nm}^{\lambda\mu})^2, \quad \Delta t = t^B - t^A .$$

We are finally left with the simple formula

$$\Delta E_{\rm ord}(\{q_h\}) = \sum_h q_h V_h , \tag{3}$$

where V_h is the EPI between an atom and its hth neighbors, and the q_h are coefficients depending on the type of ordering. Actually,

$$q_h = \frac{1}{2N}(cn_h^{BB} - c^2 n_h) ,$$

where n_h and n_h^{BB} represent the total number of pairs (or coordination number) and the number of BB pairs, respectively, at the distance d_h from the origin for a given crystalline structure.

Considering only the "d" contribution in the TBA, these interactions, for a given lattice, depend upon (a) the concentration (via the concentration-dependent self-energy of the reference medium), (b) the interatomic distance, (c) the diagonal disorder $\delta_d = (\varepsilon_B - \varepsilon_A)/\bar W$ [$\bar W$ is the average half bandwidth $\bar W = (1-c)W_A + cW_B$ where W_i are the half bandwidths of the pure constituents of the alloy], possibly on (d) the off-diagonal disorder $\delta_{nd} = (W_B - W_A)/\bar W$ in cases where bandwidths of the two components of the alloy differ substantially, and (e) the filling of the d band $\bar N_e$. Thus we have

$$V_h = \bar W V(d_h, c, \delta_d, \delta_{nd}, \bar N_e) ,$$

where

$$\bar N_e = 10\int_{-\infty}^{\bar\varepsilon_F} dE\, n_{\rm dis}(E) ,$$

$$n_{\rm dis}(E) = -\frac{1}{\pi N}\mathrm{Im}\lim_{\eta\to 0}\sum_n F_n(E + i\eta) .$$

The off-diagonal effect can be taken into account by assuming a dependence of the hopping integrals on the nature of the site occupancies[15] and by using a CPA adapted to this effect.[16] We shall summarize in Sec. III the general properties of these EPI.

III. PROPERTIES OF THE EFFECTIVE PAIR INTERACTIONS

The results obtained hereafter are based on moment arguments.[17,18] Let us first recall the method. Within the TBA it is straightforward to calculate the first few moments of the electronic density of states (DOS). Let μ_k be the moment of order k of the DOS:

$$\mu_k = \int \varepsilon^k n(\varepsilon) d\varepsilon .$$

μ_k can be calculated directly by applying the following procedure: we list all closed paths on the lattice characterized by k steps. By "step" we mean the corresponding matrix element of the Hamiltonian H expressed in the local basis, i.e., the hopping integral (or intersite step) or crystalline field integral and atomic level (or on-site step). Then the contribution of a given path is obtained by summing over orbital indices, on each site, the resulting product of matrix elements. μ_k is therefore obtained by summing over all paths

$$\mu_k = \frac{1}{5N}\mathrm{Tr}H^k = \frac{1}{5N}\sum_{n,\lambda}\langle n,\lambda \mid H^k \mid n,\lambda\rangle .$$

Thus for a pure metal, if one neglects crystalline field integrals and sets $\varepsilon_d = 0$ (ε_d is the energy of the atomic level), the second moment of the DOS is merely given by

$$\mu_2=\frac{1}{5N}\sum_{\substack{n,m,\\ \lambda,\mu}}{}' (\beta_{nm}^{\lambda\mu})^2 ,$$

where the prime on the summation means that n must be different from m.

For an alloy, a given configuration is specified in terms of moments by the paths which involve diagonal matrix elements of the Hamiltonian, expressed in Sec. II, i.e., the onsite steps ε_A or ε_B. Moreover, at least two such elements are required because terms with only a single on-site step give contribution proportional to the concentration, therefore independent of the configuration. Thus the first path depending on the configuration must include two on-site steps and two intersite steps. We conclude that the first moment which characterizes a given configuration is μ_4. In other words, for a given lattice (with one type of site in the unit cell) and for a given set of electronic parameters, the first four moment differences, associated with a difference of DOS describing a given configuration and the totally disordered state, must be equal to zero:

$$\Delta\mu_k=0, \quad k=0,1,2,3 .$$

Now if we assume that the total energy of a transition-metal alloy is principally determined by the d-band energy,

$$E_b(E_F)=\int_{-\infty}^{E_F}\varepsilon n(\varepsilon)d\varepsilon ,$$

we can define in the same way the moments Δm_n associated with the ordering energy $\Delta E(\{p_k^i\})$.

Because of the relation between Δm_k and $\Delta\mu_k$ (Refs. 19–22) in a second-order perturbation with respect to E_F,

$$\Delta m_k=-\frac{1}{(k+1)(k+2)}\Delta\mu_{k+2} ,$$

we conclude that

$$\Delta m_0=\Delta m_1=0 ,$$

and

$$\Delta m_2=-\frac{1}{30N}\sum_{\substack{n,m,\\ \lambda,\mu}}{}' \delta^2(\beta_{nm}^{\lambda\mu})^2(p_n-c)(p_m-c) ,$$

where

$$\delta=\varepsilon_B-\varepsilon_A$$

if one takes into account the expression for $\Delta\mu_4$.[17,22] This latter result is strictly identical to the one obtained from the GPM expression of $\Delta E(\{p_n^i\})$ [Eq. (2)]:[7,17,22]

$$\Delta m_2=\frac{1}{2N}\sum_{n,m}{}' (p_n-c)(p_m-c)\mu_2^{V_1(R_{nm})} ,$$

where

$$\mu_2^{V_1(R_{nm})}=-\frac{\delta^2}{15}\sum_{\lambda,\mu}(\beta_{nm}^{\lambda\mu})^2$$

is the second moment of $V_1(R_{nm})$. In fact, it is straightforward to derive a more general expression for the first nonzero moment of an EPI $V_h(R_{nm})$ where the index h defines the necessary number of steps (in terms of nonzero hopping integrals) to reach site n from site m:[9,17,22]

$$\mu_{2h}^{V_1(R_{nm})}=-\frac{\delta^2}{5(2h+1)}\sum_{\lambda,\mu}\langle n,\lambda\,|\,H_a^h\,|\,m,\mu\rangle^2 , \tag{4}$$

and

$$\mu_p^{V_h(R_{nm})}=0, \quad p=0,1,\ldots,2h-1 .$$

Referring to these moment's calculations and a powerful theorem concerning the zeros of a function,[19–22] we conclude the following. (i) The minimum number of zeros of an EPI between two sites n and m reached in h steps is equal to $2h$ inside the extremal values of the d-band filling. (ii) One can easily establish a hierarchy of EPI based on the fact that their amplitude is essentially driven by their first nonzero moment. This last quantity [see relation (4)] is easily known once the moments of the pure metal are obtained. Therefore, for an fcc lattice, one can conclude that $V_1(R_1)\gg V_2(R_2)>V_2(R_4)>V_2(R_3)$, and in the same way, for a bcc lattice, we have $V_1(R_1)>V_1(R_2)\gg V_2(R_5)>V_2(R_4)\gg V_2(R_3)$ (note that to describe correctly the electronic properties of bcc crystalline structure, one has to take into account nonzero first- and second-neighbor hopping integrals). (iii) One can define a general closest-neighbor EPI based on the fact that the variation of the first EPI with interatomic distance and topology is mainly given by the second moment of the DOS for the pure metal. As it was proved elsewhere,[11,17,22,23] because this moment does not depend strongly on the topology, it turns out that the zeros of the general EPI V_1^*, as a function of the band filling, are fixed whatever the lattice structure under consideration.

Apart from these general properties we note that the EPI depend on concentration and can even change sign in some cases over the whole concentration range $c=[0,1]$. Because of the following property: $V(c,\delta_d)=V(1-c,-\delta_d)$, the EPI are in general not symmetric with respect to $c=0.5$. All of these properties will strongly affect the shape of the phase diagram, as will be seen.

IV. SIMPLIFIED STRUCTURAL MAP

The general properties of the nearest EPI allow us to propose a simplified structural map $(c,\bar{N}_e)$ where the zeros of V_1 are reported. The position of the zeros of V_1 being roughly insensitive to the crystalline structure, we calculated the first EPI relative to fcc by the TBA-CPA-GPM. The map is presented in Fig. 1 for different values of the diagonal disorder parameter δ_d. With our conventions [see Eq. (2)], the tendency toward ordering (or phase separation) is specified by $V_1>0$ (or $V_1<0$). Since, by convention, the map is drawn for $\delta_d>0$ (i.e., $\varepsilon_B>\varepsilon_A$), we have necessarily $N_A>N_B$, i.e., A and B belong to the end and the beginning of the transition-metal series, respectively. The diagram of Fig. 1 may be used as follows: construct a straight line from N_A ($c=0$) to N_B ($c=1$), $N_A>N_B$, for the particular binary alloy system under consideration. Portions of the straight line which fall inside the central region of the map, marked "order," determine the approximate ranges of concentration where ordering takes place for that alloy system,

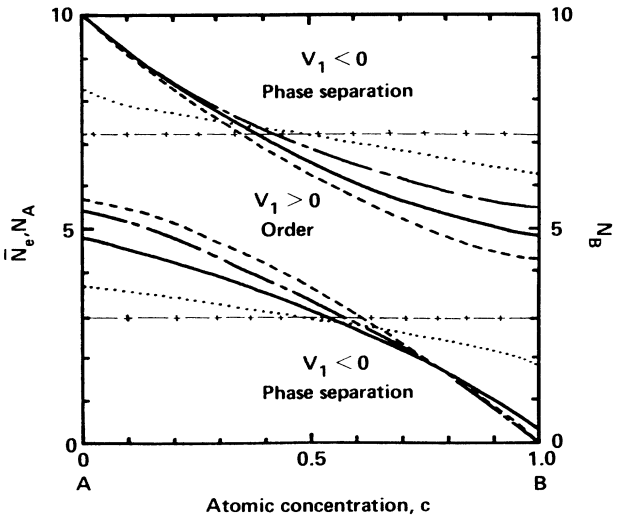

FIG. 1. Generalized structural map $(c,\bar{N}_e)$ for an $A_{1-c}B_c$ alloy and $\delta_d > 0$ (i.e., $N_A > N_B$): — — —, $\delta_d = 1.4$; ——, $\delta_d = 1.0$; —·—·—, $\delta_d = 0.6$; · · · ·, $\delta_d = 0.2$; and —+—, $\delta_d \to 0$ ($\delta_{nd} = 0.0$).

phase separation being expected elsewhere.

Figures 2(a)–2(c) show schematically how the first EPI for fcc varies as a function of concentration c, number of d electrons per atom in A and B (N_A and N_B), and the diagonal disorder δ_d.

(a) Let us first fix δ_d: Fig. 2(a) gives a measure of the influence of $\Delta N_e = N_A - N_B$ on V_1. Although the effect can be quantitatively important, the general profile behavior of $V_1(c)$ is preserved. In particular, one can note the general asymmetry of $V_1(c)$ with respect to $c = 0.5$ with a maximum of V_1 toward the higher concentration in the A element of the end of the series.

(b) Figure 2(b) shows the influence of δ_d for fixed values of ΔN_e. A decrease of δ_d implies a corresponding decrease of the maximum amplitude of V_1 without changing its location relative to the c axis. This effect can be of major importance because, as it was proved elsewhere,[24] the charge transfer effect which is not included in the present calculations generally decreases the estimated value of δ_d. Furthermore, this result is confirmed by photoemission experiments which prove that the split band case occurring for a high value of δ_d is rarely observed.[25]

(c) Finally, Fig. 2(c) illustrates the simultaneous influence of N_A and N_B for fixed values of δ_d and ΔN_e. It appears that the shift of the maximum amplitude of V_1 is strongly correlated with the average value $\frac{1}{2}(N_A + N_B)$. In other words, when this quantity is higher than five, the maximum of V_2 is located in the region $c < \frac{1}{2}$, i.e., for higher concentration in the A atom, and conversely when the average is less than five.

When concerned with particular examples, the energy unit is fixed in order to reproduce the average d-band width of the alloy under consideration. In the present study the values of the Slater-Koster parameters [$(dd\delta) = -1.385$, $(dd\pi) = \frac{1}{2}|(dd\sigma)|$, $(dd\delta) = 0$], which are quite consistent with those obtained from various interpolation schemes, give for the fcc DOS a d-band width of 11.08 in canonical units (c.u.). Because of the spin degeneracy and the number of d orbitals, a factor of 10 must be taken into account. In conclusion, for a typical bandwidth of 5 eV, the energy scale is thus given by 1 c.u. $\approx$ 4.5 eV. This scale, driven by the set of Slater-Koster parameters, will be kept fixed in the following sections.

To summarize this section, we claim that the GPM, derived from electronic structure calculations, is well adapted to give a convergent expansion of the ordering energy

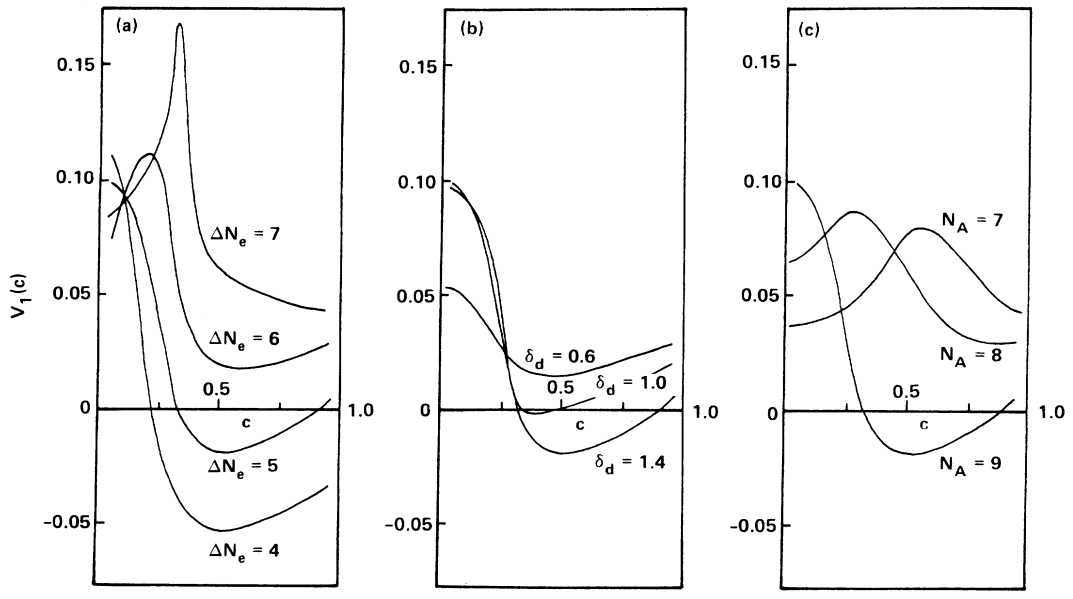

FIG. 2. Variation of the first-neighbor effective pair interaction V_1 (expressed in canonical unit c.u.), for an fcc crystalline structure, as a function of the atomic concentration c: (a) $N_A = 9$ and $\delta_d = 1.4$; (b) $N_A = 9$ and $\Delta N_e = 5$; (c) $\Delta N_e = 5$ and $\delta_d = 1.4$ ($\delta_{nd} = 0.0$).

in terms of effective pair and, more generally, cluster interactions. The rapid convergence in real space of such an expansion is ensured as long as the concentration dependence of the effective interactions is taken into account. By a moment analysis, one can deduce that in most of the cases only the first EPI are significant. The general properties of the nearest EPI, among others, allow us to propose a simplified structural map which gives the tendency toward ordering or phase separation for a given alloy. This kind of map already had been used to obtain reliable results for the relative stability of ordered superstructures constructed on the same underlying lattice[7,8,17] or on different ones.[11,17] The implicit results contained in such maps show that the influence of electronic parameters on the behavior of the nearest EPI as a function of c is actually well understood[23] and exhibit general qualitative features which will be of major importance for detailed study of phase diagrams. Finally, this approach is quite general and the GPM can be developed not only within a simple tight-binding model but also using more sophisticated methods, such as the KKR-CPA (Refs. 26 and 27) to describe more accurately the electronic structure of the reference medium. Moreover, the formalism can be easily extended to the study of correlative effects of chemical and magnetic orders[28] and also of the relative stability of multicomponent alloys.

V. FREE ENERGY

Calculation of the free energy for a given alloy system in the present context proceeds as follows: First, a number of different crystalline structures (fcc, bcc, etc.) are selected. For each lattice type, band-structure calculations are performed over the whole concentration range $c=[0,1]$, assuming complete configurational disorder. Each lattice type is associated with a set of ordered superstructures (also called the ground states), their number and complexity being given from the search of the ground states of the Ising model which is solved for a particular set of effective interactions, the same as the one retained in the GPM expansion. The resulting phase diagram, of course, will contain only those phases which have been explicitly included in the calculation.

Formally the free energy per lattice point of a binary alloy for a given phase (superstructure α) built on a given crystalline structure (I) can be written as

$$F^{I_\alpha}=(1-c)F_A^I-cF_B^I+\Delta E_m^{I_\alpha}-T\Delta S_m^{I_\alpha} , \tag{5}$$

where $F_i^I=E_i^I-TS_i^I$ is the free energy per atom of the element i ($i=A,B$) with the crystalline structure I, with E_i^I and S_i^I denoting energy and entropy, respectively, of the i species.

The formation energy $\Delta E_m^{I_\alpha}$ consists of several contributions. Some of these are related to atomic displacements, both static (elastic and relaxation energies) and dynamic (lattice vibrations). In this preliminary study, however, atoms will be regarded as rigidly confined to their ideal lattice positions, so that elastic, vibrational, and volume change contributions to $\Delta E_m^{I_\alpha}$ will be neglected. It will also be assumed that the change in vibrational entropy upon ordering (on a rigid lattice) is negligible compared to the configurational entropy change. The latter is then regarded as the only contribution to the entropy of mixing $\Delta S_m^{I_\alpha}$, and with the same kind of assumptions S_i^I will be neglected.

Within the stated hypotheses, the energy of mixing is then

$$\Delta E_m^{I_\alpha}=E_{\rm dis}^I-E_{\rm lin}^I+\Delta E_{\rm ord}^{I_\alpha} , \tag{6}$$

where $E_{\rm lin}^I=(1-c)E_A^I+cE_B^I$ is the linear interpolation between the cohesive energies of the pure elements for the reference lattice of type I, $E_{\rm dis}^I$ is the cohesive energy (for the same lattice I) of the completely disordered state, as calculated within the CPA, and $\Delta E_{\rm ord}^{I_\alpha}$ is the configurational part of the mixing energy which can be expanded, as it was shown in Sec. II, in terms of effective interactions. As a first step, this contribution is given by [see Eq. (3)]

$$\Delta E_{\rm ord}^{I_\alpha}=\sum_h q_h^{I_\alpha}V_h^I .$$

Such a decomposition of the total free energy shows that it will be much more difficult to calculate phase stability diagrams than to determine the phase stability conditions for homogeneous ordered structures (or structural maps) at $T=0$ K. Indeed, the structural maps depend essentially on the relative values of mixing energies whereas a phase diagram is determined by the different contributions to the free energy in the entire range of concentration; for example, a slight modification in $\Delta E_m(c)$ can lead to a change of stability of an ordered structure compared to a mixing of ordered or disordered phases at other concentrations.

In the present exploratory study, we shall limit our investigation to the influence of concentration-dependent pair interactions and disordered energies on the resulting phase diagrams by considering only one crystalline lattice, at present the fcc lattice. This restrictive framework allows us to consider the following free-energy expression:

$$\Delta F_m^\alpha=\Delta E_m^\alpha-T\Delta S_{\rm conf}^\alpha , \tag{7}$$

where $\Delta S_{\rm conf}^\alpha$ is the configurational entropy relative to superstructure α. (We have now no more need for a roman number because all the quantities are referred to the same lattice type.) Note that since phase equilibria are unaltered when the same linear function of concentration is added to the free energy of all phases, the linear terms in Eq. (5) may be discarded, as they are seen not to depend on the ordered phase index α. In comparing, say fcc and bcc related phases, then the linear terms play an important role and must be retained as will be shown in a future study. In order to set up the practical expression of the total free energy, let us rewrite it in a way consistent with the basic CVM equation.[1,29,30] At first, it is preferable to introduce the occupation number σ_n which, in the case of a binary alloy, can take two values ±1 depending on the site occupancy.[29] σ_n is related to p_n, previously introduced, by the relation $\sigma_n=2p_n-1$. So now a given configuration is specified at $T=0$ K by the set $\{\sigma_n\}$, and the ordering energy in the EPI approximation is given by

$$\Delta E^{\alpha}_{\rm ord}(c,T)=\tfrac{1}{4}\sum_{s}\sum_{r}\gamma^{\alpha}_{s,r}V_s(c)\delta\xi^{\alpha}_{s,r}(c,T)\ , \tag{8}$$

where s is the coordination shell index and r denotes a type of pair. The latter index is required because, in the ordered superstructure α, various s-neighbor pairs are no longer necessarily equivalent, as they are in the disordered phase. In Eq. (8) $\gamma^{\alpha}_{s,r}$ stands for the number per unit cell of s-neighbor pairs of type r in the α superstructure (in the disordered phase, this number is half the coordination number, i.e., $n_s/2$) and $\delta\xi$ is the difference:

$$\delta\xi^{\alpha}_{s,r}=\xi^{\alpha}_{s,r}-\xi^{R}_{s} \tag{9}$$

between correlation functions in the (partially) ordered phase α, and the completely disordered (superscript R for random) state, which is the reference medium used in the calculation of $E_{\rm dis}$. The pair correlation functions themselves are obtained from the ensemble average:

$$\xi^{\alpha}_{s,r}=\langle\sigma_n\sigma_{n+s}\rangle^{\alpha}_{r}\ . \tag{10}$$

Since there are no site occupation correlations in the completely random state, the expectation values of pair correlations ξ^{R}_{s} is simply related to the concentration by

$$\xi^{R}_{s}=(\Delta c)^2\ , \tag{11}$$

where

$$\Delta c=c_B-c_A=2c-1\ .$$

In contradistinction to usual mean-field theories, the correlation functions ξ are temperature dependent, and so, therefore, is the ordering energy, as indicated in Eq. (8), since the degrees of short and long range may vary with temperature in each phase. Thus, as announced, a very convenient decoupling of state of order (hence, of temperature) and of electronic calculations is achieved by the GPM: $E_{\rm dis}(c)$ and $V_s(c)$ do not depend on the superstructure type (index α), nor on the temperature, and are thus calculated before being entered into the free-energy expression (7), while the $\xi^{\alpha}_{s,r}$ are determined (i) by the symmetry of the α superstructure considered and (ii) by minimizing the CVM free energy.

The CVM free energy itself is constructed by adding to the energy ΔE^{α}_{m}, defined above [see Eq. (6)], the term $-T\Delta S^{\alpha}_{\rm conf}$, where the CVM configurational entropy is given by[1,29–34]

$$\Delta S^{\alpha}_{\rm conf}=-k_B\sum_{m,r}\gamma^{\alpha}_{m,r}a_m\operatorname*{Tr}_{\zeta}\rho_{m,r}(\zeta)\ln\rho_{m,r}(\zeta)\ , \tag{12}$$

where k_B is Boltzmann's constant, and where the summation is over clusters of m lattice points of type r included in the maximum cluster which defines the order of the CVM approximation, $\gamma^{\alpha}_{m,r}$ being the number of such clusters per lattice point in structure α [these numbers represent a generalization of the ones introduced in Eq. (8)], a_m are the Kikuchi-Barker coefficients[35,36] whose algebra is defined elsewhere[30] and the trace is over all configurations (ζ) of the partial density matrices:[30,33]

$$\rho_{m,r}(\zeta)=\frac{1}{2^m}\left[1+\sum_{m',r'\subset m,r}v^{\alpha}_{m',r';m,r}(\zeta)\xi^{\alpha}_{m',r'}\right]\ , \tag{13}$$

where the v^{α} are elements of the so-called "v matrix" or "configuration matrix" whose elements are given by sums of products of the σ_p.[31,34] In Eq. (13) the summation is over all subclusters (m',r') of the cluster (m,r) considered. In Eq. (13) the general term $\xi^{\alpha}_{m',r'}$ is a multisite correlation function defined as the ensemble average of the product of m' occupation numbers associated with the respective m' points of the cluster of type r' of superstructure α [i.e., a generalization of Eq. (10)]. A slight difference in the meaning of the subscripts pertaining to the correlation function introduced in Eqs. (8) and (13) has to be noted.

The phase diagram computations proceed by inserting Eqs. (6) and (12) into (7), making use of (8)–(11) and (13), and minimizing the resulting free-energy functional ΔF^{α}_{m} with respect to its independent variables, for each superstructure α. For the case of a (partially) ordered phase, because the long-range order (LRO) is described by means of sublattices, the point correlation functions $\{\xi^{\alpha}_{1,r}\}$ are replaced by $\xi^{R}_{1}=\Delta c$ and the LRO parameter η (several parameters in some cases), which corresponds to the amplitude of the characteristic concentration waves which determine a particular type of order, following for that purpose the prescription largely commented upon elsewhere.[1,37]

After the transformation

$$\{\xi^{\alpha}_{1,r}\}\rightarrow\{\xi^{R}_{1},\eta^{\alpha}\}$$

is performed, because the energy parameters themselves are concentration dependent, the minimization must be carried out at constant concentration, i.e., in a canonical rather than grand canonical scheme [see the implicit formulation of Eq. (7)]. According to this variational procedure, the free energy is minimized by using a modified version of the Newton-Raphson iteration scheme, with respect to the LRO parameter(s), pair and multisite correlation functions, the concentration (or ξ^{R}_{1}) being kept constant. The correlation functions $\{\xi^{*}\}$ obtained after minimization, when reinserted into ΔF^{α}_{m}, yield the equilibrium free energy $\Delta F^{\alpha *}_{m}(c,T)=\Delta F^{\alpha}_{m}(\{\xi^{*}\},cT)$ and the $\{\xi^{*}\}$ themselves provide values of short- and long-range order parameters and all subsequent information such as cluster concentrations.[38] The computation is repeated for an appropriate number of concentrations c and for several temperatures. Phase equilibrium at given T is determined by constructing lowest common tangents between free-energy curves for the different phases (α) considered.

For computational purposes, it is preferable to use a scheme devised by Kikuchi[39] which consists in looking for intersections of the Legendre transform of the free energy, i.e., the "grand potential"

$$G^{\alpha}=F^{\alpha}-\Delta\mu^{\alpha}\Delta c\ ,$$

where $\Delta\mu^{\alpha}$ is the difference in chemical potentials $\mu^{\alpha}_{B}-\mu^{\alpha}_{A}$, obtained by taking the following partial derivative:

$$\Delta\mu^{\alpha}=\frac{\partial F^{\alpha}}{\partial\Delta c}\ .$$

VI. PHASE DIAGRAM COMPUTATION

As a means of testing the methods described above, preliminary calculations were performed on a rigid fcc lattice in the EPI approximation. Since the first-neighbor pair is expected to be more influent than high-neighbor pairs for typical binary paramagnetic transition-metal alloys, the first EPI, V_1, alone was calculated by the GPM and inserted in the nearest-neighbor tetrahedron approximation of the CVM, which represents the basic improvement of the configurational entropy calculation compared to what is obtained within the Bragg-Williams approximation. From the studies related to the search of the ground states of the Ising model with just V_1, we have to consider two superstructures: $L1_2$ (Cu_3Au type) and $L1_0$ (CuAu type) beside the disordered state.[12,13]

The TB-CPA calculations were performed with the canonical values of the Slater-Koster parameters mentioned in Sec. IV. As a consequence, the temperature scale is fixed by the following expression:

$$T(K)=\frac{1.602\,19\times10^{-15}}{1.380\,62\times10^{-23}}\frac{10\overline{W}}{11.08}T(\text{c.u.}) ,$$

which gives for a typical value of average bandwidth equal to 5 eV

$$T(K)\sim 52\,370T(\text{c.u.}) .$$

Calculated curves for V_1 and $\Delta E_{\text{dis}}=E^I_{\text{dis}}-E^I_{\text{lin}}$ [see Eq. (6)] as a function of c are shown in Figs. 3(a) and 3(b), respectively, for selected sets of alloy parameters N_A, N_B, and δ_d. As expected when $N_A+N_B=10$, the $V_1(c)$ curves peak around the central concentrations whereas for $N_A=9$ and $N_B=3$, the V_1 curves are asymmetric and peak towards the A element. In all cases, the amplitude of the $V_1(c)$ profiles increases as δ_d increases. Values of $\Delta E_{\text{dis}}(c)$ and $V_1(c)$ are then inserted into the appropriate terms of the free-energy functional ΔF_m. In Table I we give the number of correlation functions and the coefficients we need to calculate the different contributions to ΔF_m. In particular, the ordering energies for the three possible fcc-related phases are given by

$$\Delta E_{\text{ord}}=\begin{cases}\frac{1}{4}[\xi_{2,1}+4\xi_{2,2}+\xi_{2,3}-6(\Delta c)^2]V_1(c) & \text{for } L1_0 ,\\ \frac{1}{4}[3\xi_{2,1}+3\xi_{2,2}-6(\Delta c)^2]V_1(c) & \text{for } L1_2 ,\\ \frac{3}{2}[\xi_{2,1}-(\Delta c)^2]V_1(c) & \text{for the fcc disordered phase} ,\end{cases}$$

whereas the configurational entropy $\Delta S^{\alpha}_{\text{conf}}$ is simply given by relation (12) in the nearest-neighbor fcc tetrahedron approximation of the CVM by making use of Table I.

Phase diagrams associated with $N_A=9$ and $N_B=3$, $N_A=7$ and $N_B=3$ (named hereafter, for short, 9-3 and 7-3 systems, respectively) have been calculated as a function of the diagonal disorder parameter δ_d which has been given the values 0.6, 0.8, and 1.0 in order to cover the two extreme cases of overlap and split band regimes of the disordered DOS. A 9-4 system with $\delta_d=0.8$ has been added for completeness. The shape of one particular phase diagram will be explained in detail by studying the variation of the free-energy contributions with respect to concentration for a series of temperatures. This examination will allow us, in Sec. VII, to extract some general trends linking the $\Delta E_{\text{dis}}(c)$ and $V_1(c)$ curves to the shape of a phase diagram. In all cases, the order-disorder transitions are found to be first order.

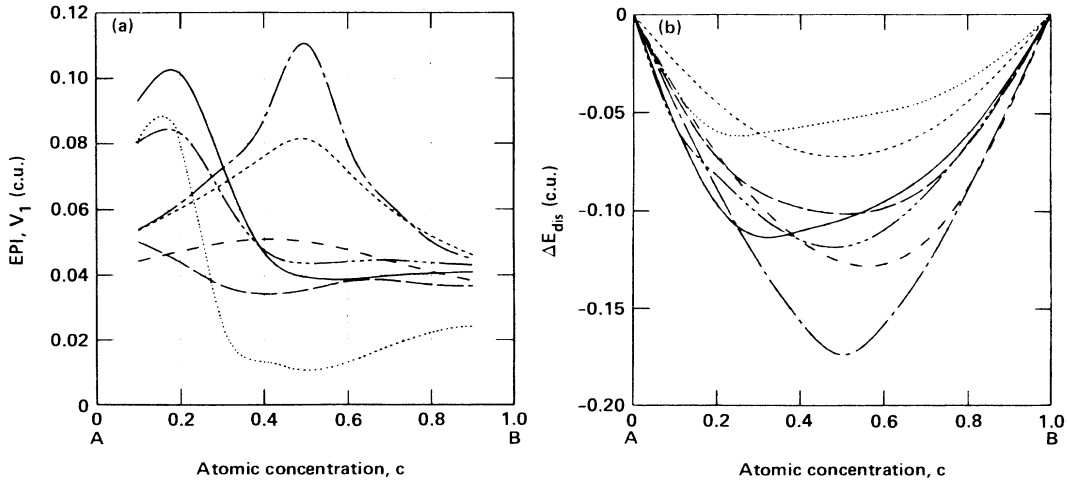

FIG. 3. Calculated first-neighbor effective pair interaction V_1 (a) and mixing energy $\Delta E_{\text{dis}}(b)$ (both expressed in canonical unit c.u.), as a function of the atomic concentration c for an fcc crystalline structure with the following alloy parameters: ——, $N_A=9$, $N_B=3$, and $\delta_d=1.0$; — - - - —, $N_A=9$, $N_B=3$, and $\delta_d=0.8$; ——, $N_A=9$, $N_B=3$, and $\delta_d=0.6$; —·—·-, $N_A=7$, $N_B=3$, and $\delta_d=1.0$; - · -, $N_A=7$, $N_B=3$, and $\delta_d=0.8$; — — —, $N_A=7$, $N_B=3$, and $\delta_d=0.6$; · · · ·, $N_A=9$, $N_B=4$, and $\delta_d=0.8$ ($\delta_{nd}=0.0$).

TABLE I. Parameters needed to describe tetrahedron clusters in $L1_0$, $L1_2$, and the fcc disordered state. The first column gives the list of subclusters for each phase. The m and r indices specify the correlation functions $\xi^{\alpha}_{m,r}$, (m and r stand for number of lattice points in the cluster and the type of cluster, respectively).

$L1_0$				$L1_2$				fcc disordered state			
m	r	γ	a	m	r	γ	a	m	r	γ	a
• 1	1	1	5	• 1	1	1	4	• 1	1	1	5
○ 1	2	1	5	○ 1	2	3	5	— 2	1	6	−1
•–• 2	1	2	−1	•–○ 2	1	12	−1	△ 3	1	8	0
•–○ 2	2	8	−1	○–○ 2	2	12	−1	⟠ 4	1	2	1
○–○ 2	3	2	−1	○–○ 3	1	24	0				
•–• 3	1	8	0	○–○ 3	2	8	0				
○–○ 3	2	8	0	○–○ 4	1	8	1				
○–○ 4	1	4	1								
$\eta=\frac{1}{2}(\xi_{1,1}-\xi_{1,2})$				$\eta=\frac{1}{2}(\xi_{1,2}-\xi_{1,1})$							
$\xi_1^R=\frac{1}{2}(\xi_{1,1}+\xi_{1,2})$				$\xi_1^R=\frac{1}{4}(\xi_{1,2}+3\xi_{1,1})$							

(a) *9-3 system.* Figures 4(a)–4(c) show the influence of δ_d on the shape of the resulting phase diagram for the 9-3 system. At a high δ_d value, $\delta_d=1.0$ [see Fig. 4(a)], a pronounced asymmetry in the phase diagram towards the low concentration in B species and a huge miscibility gap (MG) involving the disordered state at two different concentrations are prominent features of the diagram. Two spinodal curves are obtained which correspond to the ⟨100⟩ ordering and the ⟨000⟩ clustering cases. The concept of spinodal line was explained in detail elsewhere (see, e.g., Refs. 1 and 40). The occurrence of a spinodal line is associated with the cancellation of the determinant of second derivatives of the free energy with respect to the set of independent correlation functions. One can check

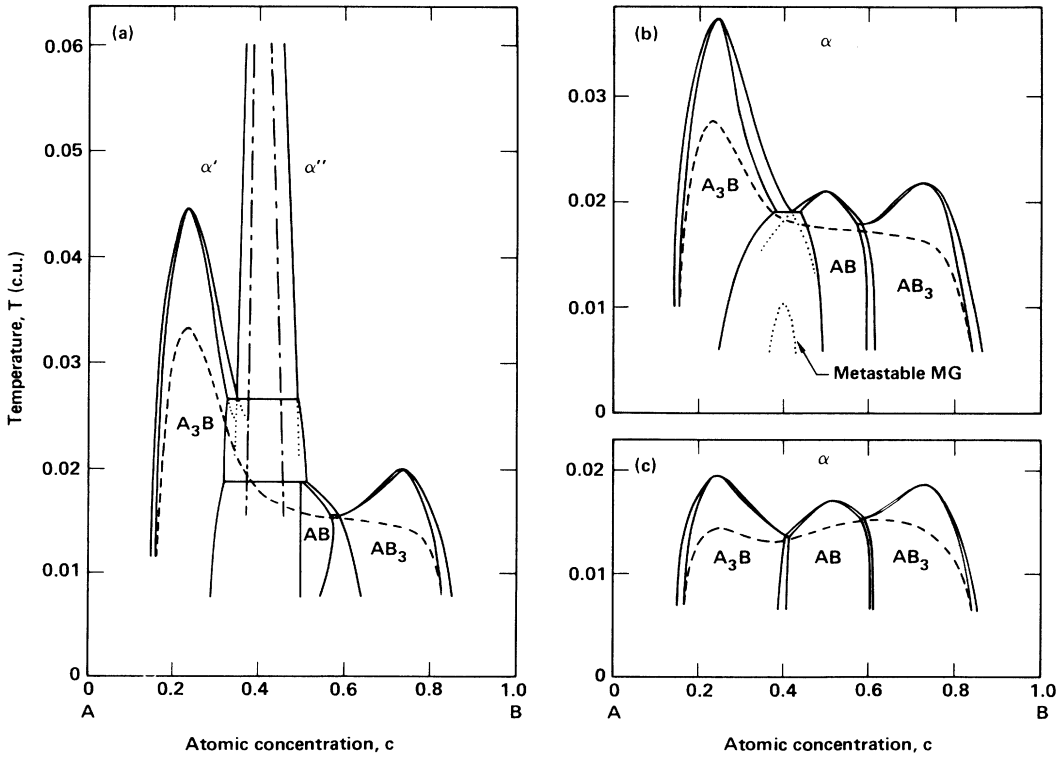

FIG. 4. Equilibrium fcc order-disorder phase diagrams calculated with the tetrahedron approximation of the CVM using the energy data for $N_A=9$, $N_B=3$ [see Figs. 3(a) and 3(b)], and (a) $\delta_d=1.0$; (b) $\delta_d=0.8$; (c) $\delta_d=0.6$ ($\delta_{nd}=0.0$). The dashed-dotted and dashed lines correspond to the ⟨000⟩ clustering and ⟨100⟩ ordering spinodal curves, respectively, whereas the dotted lines indicate some of the metastable equilibria. A_3B and AB_3 correspond to the $L1_2$ ordered phase, AB to the $L1_0$ ordered phase, and α stands for the fcc disordered state (T is expressed in canonical unit c.u.). In (b) a metastable MG involving the disordered state at two different concentrations is also mentioned.

that the maximum value of the ordering temperature T_c when it is located at stoichiometry, is related to the value of V_1 as follows:

$$4kT_c = \tau V_1 ,$$

where, in the fcc-tetrahedron approximation of the CVM, the constant τ takes the value 1.9248 and 1.8924 for the $L1_2$ and $L1_0$ order-disorder transitions, respectively. This result shows how the CVM is relevant when compared to what is obtained by Monte Carlo simulation for which $\tau = 1.766$.[38]

For this particular value of δ_d ($\delta_d = 1.0$), Figs. 3(a) and 3(b) exhibited a marked asymmetry in the $V_1(c)$ curve and an almost linear region in the $\Delta E_{\rm dis}(c)$ curve. These features turn out to have a significant influence on the free-energy contributions $\Delta E^{\alpha}_{\rm ord}, -TS^{\alpha}_{\rm conf}$ (and therefore $\Delta E_{\rm dis}$) which result in the phase diagram of Fig. 4(a). At high temperature, $T=0.120$ c.u., the disordered state is the only stable phase. Because of the still existing short-range order (SRO), $\Delta E_{\rm ord}$, although small, differs from zero [see Fig. 5(a)] with a maximum value in the vicinity of $c=0.25$ associated to the maximal value of V_1 in the same range of concentration. The $-TS$ curve has a large amplitude in agreement with the high temperature and the resulting high disorder. The degree of disorder (or the SRO parameter) comes close to complete randomness as is illustrated by the comparison of the $-TS$ curve and the one deduced from the Bragg-Williams approximation: $-kT\,[c\ln c + (1-c)\ln(1-c)]$ [see Fig. 5(a)]. The $\Delta E_{\rm dis}$ contribution, negative in the whole range of concentration, which indicates a clear tendency to alloy formation, shows an almost linear behavior around $c=0.4$ [see Fig. 3(b)]. Although the second derivative of $\Delta E_{\rm dis}$ with respect to concentration is minimal in this range of concentration, this feature does not show up in the ΔF_m curve because of the pronounced convexity of the $-TS$ curve.

At $T=0.063$ c.u. the concavity of $\Delta E_{\rm ord}(c)$ around $c=0.4$ [see Fig. 5(b)], which cannot be counterbalanced by the $-TS$ behavior results in the same effect for ΔF_m, hence leading to a MG In the phase diagram. The high value of V_1 around $c=0.25$ causes strong SRO so that the entropy is significantly less as it would be for a totally disordered state.

At $T=0.44$ c.u. [see Fig. 5(c)], long-range order sets in locally and the $L1_2$ phase manifests its existence by a first-order transition. The shift in the location of the maximum T_c towards low concentration in B species (contrary to previous calculations where V_1 is supposed to be concentration independent[1,2,41]) is easily explained by the fact that the V_1 curve itself has a sharp maximum at a concentration below stoichiometry ($c \sim 0.2$). It can also be noticed that although the $\Delta E_{\rm ord}$ curves for the ordered and the disordered states differ notably, this difference is largely compensated by the difference in the $-TS$ curves so that the resulting ΔF_m curves for both states are relatively close. The MG broadens when T decreases because the $-TS$ curve becomes less influential. Due to the jump in the LRO parameter at T_c (first-order transition-type behavior), for $T < T_c$, the configurational entropy of an ordered phase tends to zero at the stoichiometry and correspondingly the $\Delta E_{\rm ord}$ curve exhibits a sharp extremum [see Figs. 5(c)–5(e)]. At $T=0.021$ c.u. [Fig. 5(d)], the $L1_2$ range of stability broadens in such a way that the MG becomes metastable. As a result, a two phase region between $L1_2$ and the fcc disordered phase appears.

At low temperature, $T=0.013$ [see Fig. 5(e)], two other phases appears: the $L1_0$ and the $L1_2$ phases around $c=0.5$ and 0.75, respectively. In this situation four stable equilibria can be observed: *dis*-$L1_2$, $L1_2$–$L1_0$, $L1_0$–$L1_2$, and $L1_2$-*dis*, and three metastable ones have also been indicated: *dis-dis* (MG), and $L1_2$-*dis* and *dis*-$L1_0$.

The above comments clearly demonstrate a connection between the shape of the $V_1(c)$ and $\Delta E_{\rm dis}(c)$ curves and the resulting phase diagram. A small value of the second derivatives of $\Delta E_{\rm dis}$ with respect to concentration can induce miscibility gap or broad two phase regions. It has been mentioned already that the maximum temperature below which an ordered phase is found stable is propor-

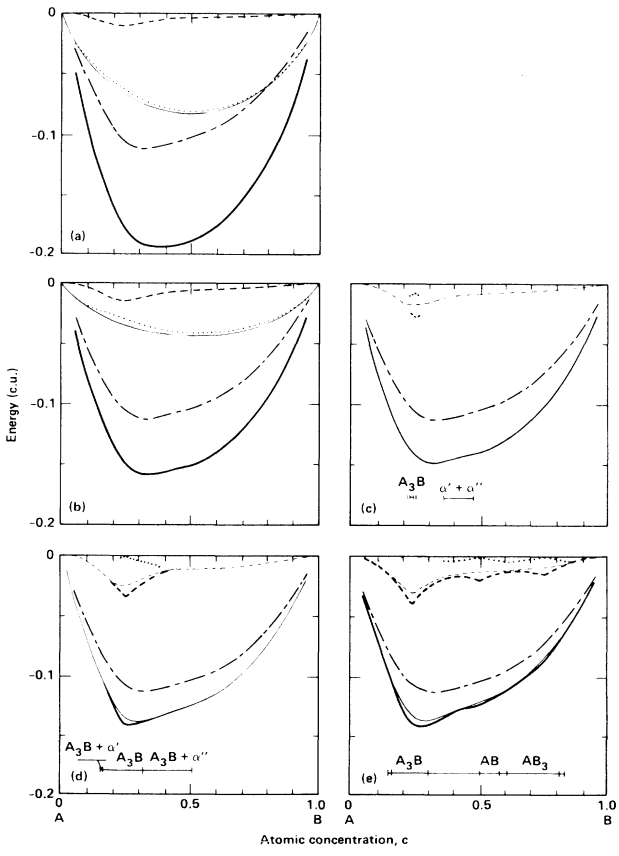

FIG. 5. Component curves of $\Delta F_m = \Delta E_{\rm dis} + \Delta E^{\alpha}_{\rm ord} - TS^{\alpha}_{\rm conf}$ for the phase diagram of Fig. 4(a) ($N_A = 9$, $N_B = 3$, $\delta_d = 1.0$, and $\delta_{nd} = 0.0$) as a function of atomic concentration c at various temperatures (expressed in canonical unit c.u.): (a) $T=0.120$; (b) $T=0.063$; (c) $T=0.44$; (d) $T=0.21$; (e) $T=0.13$. Thick and thin lines, when ambiguity exists, refer to ordered phase(s) and solid solution, respectively, with the following conventions: ——, ΔF_m; – – –, $\Delta E_{\rm dis}$; — — —, $\Delta E^{\alpha}_{\rm ord}$; · · · ·, $-TS^{\alpha}_{\rm conf}$. In (a) and (b) a thin solid line refers to $-TS^{\alpha}_{\rm conf}$ as calculated in the Bragg-Williams approximation. In (c)–(e) some of the domains of stability of the existing phases are indicated for memory.

tional to the EPI at the corresponding concentration; therefore, the shape of the $V_1(c)$ curve is reflected in that of the phase diagram.

When δ_d is equal to 0.8, the maximum of V_1 is less pronounced than in the previous case, although the overall shape is still asymmetric. These properties are transferred in the resulting phase diagram [see Fig. 4(b)]. Because the $\Delta E_{\rm dis}(c)$ curve tends to be parabolic, the MG vanishes completely. Finally, when $\delta_d=0.6$ the $V_1(c)$ curve is almost concentration independent whereas the corresponding $\Delta E_{\rm dis}(c)$ curve is well fitted by a parabola centered around $c=0.5$. This case "reduces" to the Ising model approximation, and the phase diagram [see Fig. 4(c)] resembles the one given, for example, in Refs. 1, 2, and 41. The value of T_c is again related to the amplitude of V_1. Another feature in that case is the existence of wide single phase regions.

(b) *7-3 system.* Figures 6(a)–6(c) show the phase diagrams associated to the 7-3 system for typical values of δ_d. For $\delta_d=1.0$, the $V_1(c)$ curve [see Fig. 3(a)] is roughly symmetric and shows a steep maximum around $c=0.5$; on the other hand, the $\Delta E_{\rm dis}(c)$ curve [see Fig. 3(b)] is also symmetric and exhibits a deep minimum at $c=0.5$. The quasilinearity of $\Delta E_{\rm dis}$ around $c=0.4$ and 0.6 makes, as has been shown before, the alloy system sensitive to phase separation (MG) [see Fig. 6(a)]. At lower temperature, the original MG are replaced by broad two phase regions between $L1_0$ and $L1_2$. Due to the combined effects of $\Delta E_{\rm dis}$ and V_1, the two phase region between the disordered state and $L1_2$ broadens rapidly as T decreases ($-TS_{\rm conf}$ has no more effect at low temperature). As a consequence, the $L1_2$ itself is confined to a very narrow concentration range around stoichiometry. When δ_d is decreased from 1.0 to 0.8, although the overall shape of the $V_1(c)$ curve is preserved [see Fig. 3(a)], a decrease in magnitude of V_1 around $c=0.5$ is apparent. As a result, the T_c for $L1_2$ around $c=0.25$ and 0.75 are slightly modified whereas the T_c of $L1_0$ around $c=0.5$ decreases proportionally to the decrease in magnitude of the EPI. More significant is the absence of linearity in the $\Delta E_{\rm dis}(c)$ curve [see Fig. 3(b)], and consequently, no more MG's are observed [see Fig. 6(b)] and the two phase regions between $L1_2$ and $L1_0$ narrow. Because the $V_1(c)$ and $\Delta E_{\rm dis}(c)$ curves look almost the same for $\delta_d=1.0$ and 0.8 at low concentration in A or B species, no changes are noticed regarding the extremeties of the phase diagram. Upon further decrease of δ_d to 0.6, the trends previously outlined are confirmed. The EPI is almost concentration independent [see Fig. 3(a)] and the $\Delta E_{\rm dis}(c)$ curve is well fitted by a parabola around $c=0.5$ [see Fig. 3(b)]. Consequently, the corresponding phase diagram [see Fig. 6(c)] is quite comparable to the one already calculated for the 9-3 system with $\delta_d=0.6$. Once again, the broadness of the $L1_2$-disordered two phase region, at low temperature, is caused by the quasilinearity of the $\Delta E_{\rm dis}(c)$ curve in these concentration ranges.

(c) *9-4 system.* The strong asymmetric $V_1(c)$ curve for the 9-4 system with $\delta_d=0.8$ [see Fig. 3(a)] explains the

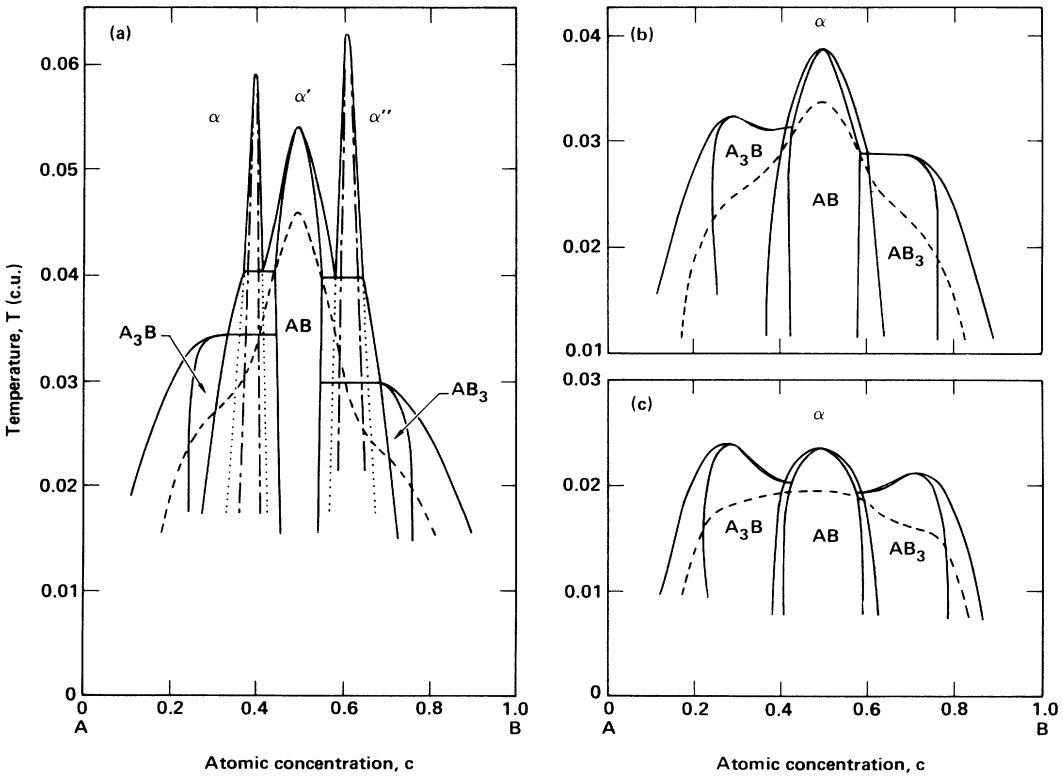

FIG. 6. Similar to Fig. 4 with the energy data associated with $N_A=7$, $N_B=3$ [see Figs. 3(a) and 3(b)], and (a) $\delta_d=1.0$; (b) $\delta_d=0.8$; (c) $\delta_d=0.6$ ($\delta_{nd}=0.0$).

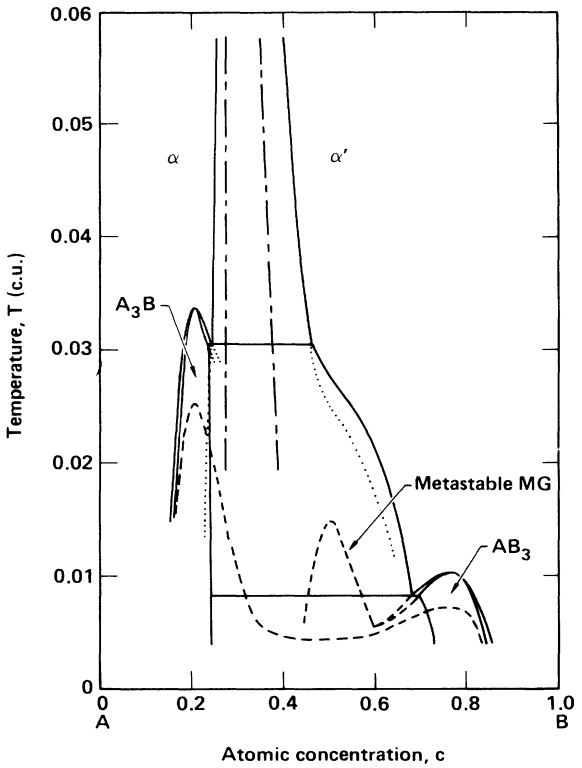

FIG. 7. Similar to Fig. 4 with the energy data associated with $N_A=9$, $N_B=4$ (see Figs. 3(a) and 3(b)], and $\delta_d=0.8$ ($\delta_{nd}=0.0$).

significant difference in the T_c values for the A_3B and AB_3 $L1_2$ phases (see Fig. 7). Due to the deep minimum of V_1 near equiatomic concentration, the $L1_0$ phase is found less stable than the $L1_2$ phases which surround it. Therefore, as a result of the minimum in $V_1(c)$ and the relative "flatness" of the $\Delta E_{\rm dis}(c)$ curve [see Fig. 3(b)], no $L1_0$ phase appears to be stable in the phase diagram. The linearity of the $\Delta E_{\rm dis}(c)$ curve around $c=0.3$ makes this system sensitive to phase separation, and the particular shape of $V_1(c)$ enhances this tendency so that a very broad MG occurs in the phase diagram (see Fig. 7).

VII. SUMMARY AND CONCLUSIONS

Because the essential physics can be derived from simple models, we considered the case of paramagnetic transition-metal alloys, the electronic properties of which can be well specified within the tight-binding approximation. By use of the GPM, when applied to the completely disordered state determined by the CPA (see Sec. II), the ordering energy can be expanded in terms of effective cluster interactions. At least as far as we are concerned with the most important terms of the expansion, i.e., the first few EPI, general properties as function of distance, concentration, and alloy parameters can be derived for them (see Sec. III), and simplified structural maps allow us to give the tendency toward order or phase separation, depending mainly on the number of valence electrons of the two components of the alloy, N_A and N_B (see Sec. IV). From that knowledge, and after focusing on the fcc crystalline structure, several values of N_A, N_B, and δ_d were selected in order to cover the typical cases of first EPI, $V_1(c)$, and mixing energy, $\Delta E_{\rm dis}(c)$, behaviors. The influence of these input data on the phase diagrams was studied by making use of the CVM to treat the statistical part of the problem correctly (see Sec. V).

Within this general framework, the present formal study (formal in the sense we did not try to apply any kind of fitting procedure to specify a particular alloy system) shows that even with a small number of concentration-dependent pair interactions (at present, just the first EPI of the fcc crystalline structure), a large variety of phase diagrams can be generated. Conversely, as far as the overall shape of an experimental phase diagram can be driven by configurational quantities, it is actually possible to learn more about stable and metastable phases. The qualitative understanding of the factors which control the appearance of the main features in a phase diagram allows us to extract the following trends. At low δ_d value, the $\Delta E_{\rm dis}(c)$ curve approximates a parabola, the $V_1(c)$ curve is almost concentration independent, and the sign of these quantities is defined by N_A and N_B. As a result, our description reduces to the Ising model formulation and *ipso facto* the phase diagram looks very similar to the fcc CVM Ising model phase diagram with quite comparable values of the order-disorder critical temperature for both types of order, i.e., $L1_2$ and $L1_0$. Upon increasing the value of δ_d, the $\Delta E_{\rm dis}(c)$ curve departs from the parabolical shape and may develop quasilinear regions which in turn make the alloy free-energy sensitive to the appearance of MG's and/or broad two phase regions. These possible effects are, in our case, driven by the configuration-dependent energy term. Because the location of the maximum value of V_1 and its magnitude are clearly defined once N_A, N_B, and δ_d are given, the importance of the gradient of V_1 with respect to the concentration allows us to predict the existence of such effects, besides the typical asymmetry of the phase diagram. Although it is still premature to compare our results with experimental phase diagrams because most of them involve incoherent and/or magnetic phases, some of the trends are confirmed. For example, the related 9-3 systems PdTi, PtTi or 9-4 systems PtNb, PtTa exhibit pronounced asymmetric phase diagrams with maximum T_c's towards the element with the greater number of valence electrons. Furthermore, most of the 7-3 alloy systems show experimentally a B2 structure which remains ordered until the melting point, generally at high temperature: RuTi constitutes in this respect a typical example. Because the first EPI (V_1 in the case of fcc, V_1 and V_2 in the case of bcc) is slightly affected by the topology of the underlying lattice, this experimental observation strongly suggests a large value of V_1 around $c=0.5$, which is in agreement with our calculations. [See also Ref. 42.]

Even in its simple version, the scheme we have been using to derive thermodynamic properties gives the correct order of magnitude for T_c. Indeed, for an average d-bandwidth of 5 eV and a V_1 around 0.05 c.u. (i.e., 225 meV), the corresponding T_c is about 1250 K. This observation encourages further studies in this direction. In particular, the results already obtained at $T=0$ K for

simple and complex structures (fcc, hcp, bcc, A15, Laves phases, etc.)[11,17] can be revisited within the present framework in order to generate incoherent phase diagrams from which more general trends will emerge, without using up excessive computing time.[42] Meanwhile, due to the different orders of magnitude involved in the calculation of the terms which make up the total free energy, it appears to be important to improve the determination of the internal energy, i.e., a more suitable reference medium (i.e., the totally disordered state) must be defined to obtain the required accuracy in the band structure calculations. This step can be achieved in two ways. The first one consists in using the TBA-CPA-GPM-CVM as an intermediate fitting procedure between *ab initio* band-structure calculations and the resulting phase diagram by including hybridization, charge transfer self consistency, and vibrational quantities.[43] The second one is to transcribe the idea of the GPM in the multiple-scattering formalism.[44] The use of the KKR-CPA equations will allow us to study a wider set of alloys, especially superalloys and other normal metal alloys which are of great technological interest.

Work in the three directions—use of crude TB model to extract tendencies for incoherent phase diagrams, refinements in the use of the TB model, and use of the first-principles band-structure calculations to derive alloy thermodynamic properties—is in progress, and will be reported in forthcoming publications. In the meantime, certain problems remain to be solved (self consistency for the calculation of the total energy, including exchange correlation and charge transfer effects, elastic interaction determination, relaxation effects, introduction of more distant interactions in the statistical models, etc.) if we are to provide truly quantitative answers to the general problem of alloy stability.

ACKNOWLEDGMENTS

This work was partially supported by a grant from the National Science Foundation. One of the authors (P.T.) was partially supported by the Department of Nuclear Chemistry, LLNL, under Contract No. W-7405-eng-48, through Dr. M. Fluss. One of the authors (P.T.) wishes to thank Dr. F. Ducastelle, Dr. A. Finel, and Professor F. Gautier for valuable discussions.

*Present address: Department of Materials Science (L-280), Lawrence Livermore National Laboratory, University of California, P.O. Box 808, Livermore, CA 94550.

[1]For a review, see D. de Fontaine, *Solid State Physics,* edited by F. Seitz, D. Turnbull, and H. Ehrenreich (Academic, New York, 1979), Vol. 34, p. 73.

[2]P. C. Clapp, Acta Metall. **22**, 563 (1974); D. de Fontaine and R. Kikuchi, Natl. Bur. Stand. (U.S.) Spec. Publ. No. SP-496 (U.S. GPO, Washington, D.C., 1978), p. 999; R. Kikuchi and D. de Fontaine, *ibid.* p. 967; J. W. Cahn and R. Kikuchi, Acta. Metall. **27**, 1329 (1979).

[3]F. Ducastelle and F. Gautier, J. Phys. F **6**, 2039 (1976).

[4]V. Heine and D. Weaire, *Solid State Physics,* edited by F. Seitz, D. Turnbull, and H. Ehrenreich (Academic, New York, 1970), Vol. 24, p. 249.

[5]J. Friedel, *The Physics of Metals,* edited by J. M. Ziman (Cambridge University Press, Cambridge, 1969), p. 340.

[6]A. Bieber and F. Gautier, Solid State Commun. **38**, 1219 (1981).

[7]A. Bieber, F. Gautier, G. Treglia, and F. Ducastelle, Solid State Commun. **39**, 149 (1981).

[8]A. Bieber, F. Ducastelle, F. Gautier, G. Treglia, and P. Turchi, Solid State Commun. **45**, 585 (1983).

[9]A. Bieber and F. Gautier, J. Phys. Soc. Jpn. **53**, 2061 (1984).

[10]A. Bieber and F. Gautier, Z. Phys. B **57**, 335 (1984).

[11]P. Turchi, G. Treglia, and F. Ducastelle, J. Phys. F **13**, 2543 (1983).

[12]S. M. Allen and J. W. Cahn, Acta Metall. **20**, 423 (1972).

[13]J. Kanamori and Y. Kakehashi, J. Phys. (Paris) Colloq. **38**, C7-274 (1977).

[14]J. C. Slater and G. F. Koster, Phys. Rev. **94**, 1498 (1954).

[15]H. Shiba, Prog. Theor. Phys. **46**, 77 (1971).

[16]A. Bieber and F. Gautier, Physica **107B**, 71 (1981).

[17]P. Turchi, Thèse de Doctorat d'Etat, University of Paris VI, 1984 (unpublished).

[18]F. Ducastelle, in *Material Research Society Symposium Proceedings,* Vol. 21 of *Phase Transformations in Solids,* edited by T. Tsakalakos (North-Holland, Amsterdam, 1984), p. 375.

[19]F. Ducastelle and F. Cyrot-Lackmann, J. Phys. Chem. Solids **32**, 285 (1971).

[20]F. Ducastelle, Thèse de Doctorat d'Etat, Université de Paris–Sud, Orsay, 1972 (unpublished).

[21]J. Dieudonné, *Calcul Infinitésimal* (Hermann, Paris, 1968), p. 162.

[22]P. Turchi and F. Ducastelle, in *The Recursion Method and Its Applications,* Vol. 58 of *Springer Series in Solid-State Sciences,* edited by D. G. Pettifor and D. L. Weaire (Springer-Verlag, Berlin, 1985), p. 104.

[23]P. Turchi and F. Ducastelle (unpublished).

[24]G. Treglia, F. Ducastelle, and F. Gautier, J. Phys. F **8**, 1437 (1978).

[25]F. U. Hillebrecht, J. C. Fuggle, G. A. Sawatzky, and R. Zeller, Phys. Rev. Lett. **51**, 1187 (1983).

[26]B. L. Gyorffy and G. M. Stocks, Phys. Rev. Lett. **50**, 374 (1983).

[27]P. Turchi, A. Gonis, and G. M. Stocks (unpublished).

[28]A. Bieber and F. Gautier, J. Magn. Magn. Mater. **54-57**, 967 1986.

[29]R. Kikuchi, Phys. Rev. **81**, 988 (1951).

[30]J. M. Sanchez, F. Ducastelle, and D. Gratias, Physica **128A**, 334 (1984).

[31]J. M. Sanchez and D. de Fontaine, Phys. Rev. B **17**, 2926 (1978).

[32]J. M. Sanchez and D. de Fontaine, Phys. Rev. B **21**, 216 (1980).

[33]D. de Fontaine, in *Modulated Structure Materials,* Vol. 83 of *Nato ASI Series, Series E: Applied Sciences,* edited by T. Tsakalakos (Martinus Nyhoff, Dordrecht, 1983), p. 43.

[34]T. Mohri, J. M. Sanchez, and D. de Fontaine, Acta Metall.

33, 1171 (1985).
[35]J. A. Barker, Proc. R. Soc. London, Ser. A **216**, 45 (1953).
[36]J. Hijmans and T. De Boer, Physica **21**, 471 (1955); **21**, 485 (1955); **21**, 499 (1955); **21**, 408 (1956).
[37]A. G. Khachaturyan, Phys. Status Solidi B **60**, 9 (1973); in *Ordering in Substitutional and Interstitial Solid Solutions*, in *Progress in Materials Science*, edited by B. Chalmers, J. Christian, and T. Massalski (Pergamon, New York, 1978), Vol. 22.
[38]T. Mohri, J. M. Sanchez, and D. de Fontaine, Acta Metall. **33**, 1463 (1985).
[39]R. Kikuchi, J. Chem. Phys. **66**, 3352 (1977).
[40]D. de Fontaine, Acta Metall. **23**, 553 (1975).
[41]C. M. van Baal, Physica (Utrecht) **64**, 571 (1973).
[42]M. Sluiter, F. Zezhong, P. Turchi, and D. de Fontaine (unpublished).
[43]C. Sigli, M. Kosugi, and J. M. Sanchez, Phys. Rev. Lett. **57**, 253 (1986), and references therein.
[44]P. Turchi, A. Gonis, and G. M. Stocks (unpublished).